Lab on a Chip

PAPER

View Article Online
View Journal | View Issue

Cite this: *Lab Chip*, 2024, **24**, 1930

AMF-SporeChip provides new insights into arbuscular mycorrhizal fungal asymbiotic hyphal growth dynamics at the cellular level†

Felix Richter,[a] Maryline Calonne-Salmon,[b] Marcel G. A. van der Heijden,[cde] Stéphane Declerck[b] and Claire E. Stanley *[a]

Arbuscular mycorrhizal fungi (AMF) form symbiotic associations with the majority of land plants and deliver a wide range of soil-based ecosystem services. Due to their conspicuous belowground lifestyle in a dark environment surrounded by soil particles, much is still to be learned about the influence of environmental (*i.e.*, physical) cues on spore germination, hyphal morphogenesis and anastomosis/hyphal healing mechanisms. To fill existing gaps in AMF knowledge, we developed a new microfluidic platform – the *AMF-SporeChip* – to visualise the foraging behaviour of germinating *Rhizophagus* and *Gigaspora* spores and confront asymbiotic hyphae with physical obstacles. In combination with timelapse microscopy, the fungi could be examined at the cellular level and in real-time. The *AMF-SporeChip* allowed us to acquire movies with unprecedented visual clarity and therefore identify various exploration strategies of AMF asymbiotic hyphae. We witnessed tip-to-tip and tip-to-side hyphal anastomosis formation. Anastomosis involved directed hyphal growth in a "stop-and-go" manner, yielding visual evidence of pre-anastomosis signalling and decision-making. Remarkably, we also revealed a so-far undescribed reversible cytoplasmic retraction, including the formation of up to 8 septa upon retraction, as part of a highly dynamic space navigation, probably evolved to optimise foraging efficiency. Our findings demonstrated how AMF employ an intricate mechanism of space searching, involving reversible cytoplasmic retraction, branching and directional changes. In turn, the *AMF-SporeChip* is expected to open many future frontiers for AMF research.

Received 10th October 2023,
Accepted 15th February 2024

DOI: 10.1039/d3lc00859b

rsc.li/loc

Introduction

Arbuscular mycorrhizal fungi (AMF) are a group of soil fungi belonging to the phylum Glomeromycota, forming a symbiosis with *ca.* 70–80% of all terrestrial plants. Laying the foundation for every soil-based ecosystem on earth,[1–3] the fungus colonises root cells (*i.e.*, the intraradical mycelium – IRM) and vastly extends into the soil (from 82 to 111 m cm^{-3} in prairie and 52 to 81 m cm^{-3} in ungrazed pasture[4]) to constitute the extraradical mycelium (ERM). This network of hyphae supplies the host plant with essential nutrients such as P and N, but also Zn, Cu and Fe,[5] and receives between 4 and 20% of the total carbon synthesised by plants in return.[6,7] Furthermore, this immensely important mutualism increases the ecosystem's overall resilience and facilitates plant productivity and plant diversity.[8] Moreover, AMF are not host specific and can interconnect different plant species forming so-called common mycorrhizal networks (CMNs).[9]

Despite their importance, much is still unknown about the influence of environmental cues on spore germination, hyphal morphogenesis, anastomosis/hyphal healing mechanisms in AMF, for example, with inoculation of crops with AMF spores in the field often failing.[10–12] This is primarily due to the fact that the study of AMF and other soil-dwellers at the cellular and sub-cellular level proves to be challenging. The opacity of soil makes it impossible to observe these organisms in their natural habitat and in real-time, rendering classic microscopy-based approaches either black-box experiments (*e.g.*, end-point microscopy) or very simplified with limited resolution.[13] The emergence, in recent decades, of *in vitro* cultivation techniques on root organs or whole plants has permitted to increase our knowledge on, for example, hyphal growth dynamics, three-dimensional architecture, anastomosis formation and hyphal

[a] *Department of Bioengineering, Imperial College London, London, SW7 2AZ, UK. E-mail: claire.stanley@imperial.ac.uk; Web: https://www.imperial.ac.uk/people/claire.stanley; Tel: +44 (0)20 75942893*
[b] *Laboratory of Mycology, Earth and Life Institute, Université catholique de Louvain, B-1348 Louvain-la-Neuve, Belgium*
[c] *Agroecology and Environment Research Division, Agroscope, 8046 Zurich, Switzerland*
[d] *Department of Evolutionary Biology and Environmental Studies, University of Zurich, 8057 Zurich, Switzerland*
[e] *Institute of Environmental Biology, Utrecht University, 3584 CS Utrecht, The Netherlands*

† Electronic supplementary information (ESI) available. See DOI: https://doi.org/10.1039/d3lc00859b

healing mechanisms.[14–16] However, the lack of vertical confinement and background of a phytagel medium restricts the microscopy quality. The membrane methods introduced by Giovannetti *et al.*[17] which involve sandwiching extraradical mycelium between Millipore or cellophane membranes[17,18] provide a confined two-dimensional system that allows for the study of cytoplasmic streaming, anastomosis formation as well as nuclear behaviours at the hyphal level. This two-dimensional confinement of the mycelium widely eliminated background hyphae, which hampered former studies, and thus improved microscopy precision and resolution. For the imaging, pieces were cut out of the sandwich cultures and results obtained from time-point microscopy. The method was further employed for the study of single spores and asymbiotic hyphae[19] where timelapse images of cytoplasmic streaming through freshly formed anastomoses were acquired.[20] In order to obtain real-time growth videos of exploring hyphae and live interactions with the environment or other hyphae, however, a system confined vertically and limited laterally, having perfect transparency, the ability to hold nutritious medium and trap spores was deemed necessary. Moreover, a major aim of this study was to explore the space-searching behaviour of AMF asymbiotic hyphae, which requires the presence of physical obstacles within the experimental platform. Although Giovannetti *et al.*[17] introduced micro-threads of different materials and diameters (10 μm to 350 μm) into their experimental system to act as non-host roots, the ability to create an array of microstructures having a defined shape and size is needed, however, to simulate more generic obstacles and particles found in soil. Therefore, a new microfluidic tool was developed to study AMF spores and asymbiotic hyphae in a visual, spatially and temporally resolved manner.

Microfluidic technology development for fungal research is a considerably young field, especially for studying hyphal behaviour and dynamics (reviewed in Richter *et al.*[21]). Being the first to explore this path, Nicolau and colleagues set out to study hyphal exploration strategies in micro-mazes, particularly with the filamentous model fungus *Neurospora crassa*.[22–25] In recent years, this was developed further to accommodate more complex studies on filamentous fungi. Thomson *et al.* and Puerner *et al.*[26,27] for instance, utilised the deformability of poly(dimethylsiloxane) (PDMS) structures to measure forces exerted by growing hyphae and Couttenier *et al.*[28] designed a device to study the effect of shear flow on hyphal bending. Further, microfluidic platforms have been developed to investigate interactions with other biological agents, such as bacteria,[29–32] nematodes,[33] bacteriophages[34] as well as fungal–fungal interactions.[35] However, only two single studies involving AMF have been published, which focus on spore sorting and extraradical hyphae.[36]

The use of microfluidic technology also allows to design microenvironments that mimic certain aspects of the natural habitat. Mafla-Endara *et al.*,[37] for example, created a soil-like microcosm featuring different geometries, species from various kingdoms, as well as water, air and soil particles as a substrate. In the course of that study, they observed how fungal hyphae help other organisms populate air-filled pockets in soil, hypothesising a water film in the mycosphere to be responsible for the transport. Further, gradients or niches of chemicals can be implemented for hyphal chemotaxis studies.[38] Ranking from highest to lowest in terms of complexity, field experiments, pot cultures and *in vitro* systems are all important experimental platforms for AMF research. Crucially, however, the microfluidics approach fills a significant experimental "gap", providing a system with a high controllability of the experimental process and precise imaging, which allows for tailored patterning of the physical, as well as chemical, environment.

Herein, we introduce a new microfluidic device, termed the *AMF-SporeChip*, that was specifically designed to accommodate spores of *Rhizophagus* species for the study of spore germination events and exploration dynamics of asymbiotic hyphae for the first time. The devices were manufactured in-house using the elastomeric polymer PDMS, which allows AMF hyphae to be confined to a single monolayer. Different micro-structures were included within the device design to mimic natural obstacles in soil (*e.g.*, mineral particles, roots *etc.*), enabling hyphal dynamics to be explored upon confrontation with physical obstacles. Owing to the material's near-perfect optical transparency, precise live imaging microscopy could be performed in real-time. To validate the compatibility of the device with AMF, we compared the germination and hyphal growth dynamics of 3 different *Rhizophagus* strains, both on-chip and on-plate, as well as demonstrating different germination behaviours between these strains. The flexibility of the system was also highlighted by (i) presenting a slightly modified device that can accommodate another AMF species, namely *Gigaspora margarita*, (ii) introducing fluorescent dyes (FM4-64 and calcofluor white) into the microchannels for staining hyphae and (iii) demonstrating the suitability of the *AMF-SporeChip* for monitoring anastomosis formation in *Rhizophagus*. As a key result, we present an interesting and so far undescribed insight concerning reversible cytoplasmic retraction within asymbiotic hyphae, which amongst hyphal branching and directional changes, we consider part of their space searching strategy.

Experimental

Chicory root and AMF culture

Three AMF strains, *i.e.*, *Rhizophagus irregularis* MUCL 41833, *Rhizophagus irregularis* MUCL 43194 and *Rhizophagus intraradices* MUCL 49410, were provided by the Glomeromycota *in vitro* collection (GINCO, Belgium). The fungi were maintained in bi-compartmented Petri plates on Ri T-DNA transformed roots of chicory (*Cichorium intybus* L.). The roots were provided by the Glomeromycota *in vitro* collection (GINCO, Belgium) and cultivated on modified Strullu and Romand (MSR) medium,[39] stored at 27 °C in the dark in an inverted position and subcultured monthly. Spores of *Gigaspora margarita* BEG 34 were produced in pots with *Plantago lanceolate* as host.[39,40] For

more information and media preparation see the ESI† (Methods).

Microfluidic device fabrication

The device designs were drawn in AutoCAD 2022 (Autodesk) and checked for correct structuring using KLayout.[41] The design was then printed to create a Mylar® film photolithography mask by Micro Lithography Services Ltd., UK. Using these photomasks, two-layered master moulds were manufactured in a clean room (detailed in ESI† Methods).

To facilitate removal of the PDMS layer from the master moulds when casting devices, the wafers were silanised, *i.e.*, made more hydrophobic. Therefore, the masters were carefully cleaned with an air gun and placed into a desiccator. In the centre of the desiccator, a glass vial containing 100 μl chlorotrimethylsilane (redistilled ≥99%, Sigma Aldrich, UK; hazardous substance, consult safety data sheet of supplier) was placed. Using a vacuum pump, the desiccator was evacuated for 1 min and then closed off. The master moulds were left to react with the chlorotrimethylsilane for 1 h.

Using the master moulds, microfluidic devices can be produced on demand. All of the following steps were conducted in a laminar flow hood. Firstly, PDMS is mixed in a 10 : 1 ratio of base to curing agent (Sylgard 184, Dow Corning, USA) and degassed for *ca.* 45 min under vacuum in a desiccator. The master mould was fitted into a frame, the PDMS poured onto it and cured overnight at 70 °C. The PDMS was then removed from the mould, cut into slabs consisting of 2 device designs and holes for the in- and outlets were punched using a cork borer (Ø = 3 mm; Syneo, USA). To remove monomer remnants and to disinfect, the PDMS slabs were washed in 0.5 M NaOH and then 70% ethanol, rinsing with sterile water between washing steps, and dried at 70 °C for 1 h. Next, the PDMS slabs as well as glass-bottomed Petri dishes (Ø dish = 35 mm, Ø glass = 23 mm; Fluorodish, World Precision Instruments, Germany) were plasma activated using a Zepto plasma cleaner (Diener Electronic, Germany; vacuum pressure 0.75 mbar, power 50%, 1 min) and bonded together, resulting in each Petri dish holding 2 devices. Exploiting the transient hydrophilicity of PDMS right after the plasma treatment, devices were filled with liquid hyphal medium (see ESI† Methods). Before use, devices were re-sterilised under UV light (254 nm) for 30 min.

Device inoculation

The spore material of *R. irregularis* MUCL 41833 and MUCL 43194, as well as *R. intraradices* MUCL 49410 was obtained directly from the above-described bi-compartmented cultures (see ESI† Methods, AMF culture). All subsequent steps were performed in a sterilised laminar flow hood, under a stereoscope (EZ4 D, Leica, Germany). Using sterilised dissection needles, spore-bearing hyphae were extracted from a culture plate that is at least 3 months old and transferred into a 90 mm Petri dish filled with liquid MSR medium lacking sucrose, termed MSR(−) (see ESI† Methods). Sterile tattoo needles (03 tight liner, pre-soldered, Barber DTS, UK) were used to cut the mycelium into smaller pieces containing 1–5 spores. Then, 5–6 of these spore pieces were transferred into each inlet of a device using a pipette (Pipetman G, 200 μl, Gilson, USA) that was set to 21 μl (to avoid overfilling of the inlets). A syringe (Henke-Ject, Luer Lock, 5 ml, HenkeSassWolf, Germany) connected to AlteSil High Strength Tubing (bore: 1.00 mm, wall: 1.00 mm, total diameter: 3 mm; Altec Extrusions Limited, UK) with a blunt tip syringe needle (1.28 mm, Shintop, China) and filled with liquid MSR(−) medium was carefully plugged into the inlet and spores were manually flushed into the device until all spores were inside of the channel and/or no more spores were coming from the inlet.

Spores of *Gi. margarita* were picked up using a pipette set to 20 μl and transferred into the inlet of the device. As the spores are detectable with the naked eye, it is easy to check visibly that only a single spore is in the pipette tip. The spores were then flushed into the device using the same method previously described for spores of *Rhizophagus*.

For staining experiments with fluorescent dyes, calcofluor white (to a final concentration of 0.5 μM) and FM4-64 (to a final concentration of 5 μM) were added to autoclaved liquid MSR(−) medium, sterile filtered and used to fill the microchannels as described above.

Image analysis and quantification

Time-lapse images (used to produce growth and germination videos) as well as time-point large images (used for measuring growth rates) were obtained with two inverted microscopes (Eclipse Ti-U and Eclipse Ti-2, Nikon; ESI† Methods). Microscopy images were processed and analysed with Image J (Fiji).[42] To measure hyphal growth, the segmented line and measurement tool were used. The measured lengths were grouped into 5 intervals; 0.1–0.4 mm, 0.5–1.0 mm, 1.1–2.0 mm, 2.1–3.0 mm and >3 mm, and represented as stacked column diagrams using Origin 2021 (OriginLab). To account for the variation in number of spores loaded into the devices, the results were normalised. Therefore, the number of germination sites (instead of the number of spores) was determined and the absolute value of counts divided by the number of germination sites. For the hyphal growth behaviour, we counted sites where a germination within 14 days of inoculation occurred as germination sites. For calculation of the germination rates, we defined any site where usually a germination occurs from, *i.e.*, cut ends of hyphal remnants, as a germination site. Germinations were counted at the last day, day 14, of the experiment. For determining significant differences in the data points for germination rates and spore distribution within devices, 1-way ANOVA was performed in Origin 2021 (OriginLab).

$$\text{Normalised count} = \frac{\text{Total count of hyphae}}{\text{Number of germination sites}}$$

Results

Design and operation of the *AMF-SporeChip*

The *AMF-SporeChip* was designed to accommodate spores of different *Rhizophagus* strains, to enable high resolution dynamic imaging of spore germination and hyphal morphogenesis events at the cellular level. A two-dimensional (2D) sketch of the microchannel architecture is displayed in Fig. 1a, which features an inlet (Ø = 3 mm) connected to a "primary spore trapping region" (microchannel height = 100 μm) that then transitions into an "investigation zone" (microchannel height = 10 μm), with a total device length of 12.4 mm. The "investigation zone" also constitutes a "secondary spore trapping region". Fig. 1b and c illustrate an overview of the *AMF-SporeChip*, where the change in microchannel height can be clearly evidenced *via* the addition of a fluorescein-containing solution, as well as how tubing is fitted into the device inlet for the introduction of AMF spores. The step change in microchannel height results in trapping of the AMF spores (Fig. 1d), which usually have a diameter on the order of 10–100 μm for *R. irregularis* MUCL 41833, 20–160 μm for *R. irregularis* MUCL 43194 and 20–120 μm for *R. intraradices* MUCL 49410 (measured, Fig. S1†), and importantly allows the much smaller, asymbiotic hyphae (Ø = 2–12 μm; measured, Fig. S2†) to access (*i.e.*, grow into) and be confined within the investigation zone in the *z*-direction.

As PDMS is an elastomeric polymer and therefore flexible in nature, the microchannel widens slightly upon applying positive pressure when using a syringe to introduce spores into the *AMF-SporeChip*.[43] Hence, some spores can be pushed into the investigation zone. Upon removing the applied pressure, the microchannel resumes its original state, thus trapping spores between top and bottom of the microchannel. Approximately 50% of introduced spores were trapped in the primary spore trapping region and 40% in the first half of the secondary spore trapping region, *i.e.*, just after the transition in channel height; a small number of spores (*ca.* 10%) got flushed into the second half of the secondary spore trapping region (Fig. 1f). The distribution in the individual device depends on many factors, such as spore size, size of the spore-cluster, length of hyphal remnants/subtending hyphae, applied pressure for device loading (due to manual loading) *etc.* A significant difference in the trapping behaviour could be observed between the obstacle-type devices and the lane-type devices (Fig. 1f). Due to the larger contact area between PDMS and glass bottom near the channel height transition, the expandability of the PDMS channels was reduced in the lane-type devices, thus making it more difficult for spores to enter the investigation zone. For spores of *Gi. margarita* (Ø = 380–580 μm; measured, Fig. S1†), the microchannel height of the inlet and spore trapping region was adjusted from 100 μm to *ca.* 350 μm. The aforementioned flexibility of the PDMS allows spores bigger than 350 μm to be accommodated within the trapping region of the microdevice, however not in the investigation zone.

The investigation zone contains an array of obstacles designed to provoke hyphal collision events (Fig. 1a). One advantage of the *AMF-SporeChip* is that the investigation zone can be modified in a bespoke manner to accommodate different types of physical obstacles that vary in their shape and size (*i.e.*, obstacle-type devices, Fig. 1e), or even possess lanes containing dead-ends or bottlenecks (*i.e.*, lane-type devices, Fig. 1e). With our choice of obstacles, we aimed to confront AMF with a variety of physical challenges that may be experienced within a soil environment. The obstacle-type devices varied in form, ranging from shapes that are either closed (circle) or open (Pac-Man, open-box, restricted open-box), therefore affording different internal angles and numbers of contact interfaces and thus offering increased or reduced chances for hyphae to "escape" from an obstacle (Fig. S3†). As expected, the restricted open-box and the dead-end lane designs seemed to be the most challenging to escape from, however, the hyphal behaviours varied widely, some hyphae managed to escape from a restricted open-box obstacle, while others failed to circumnavigate the circular shapes, and a clear pattern or obstacle dependence could not be determined. For measuring germination and growth dynamics, we utilised all designs equally to investigate how AMF hyphal tips react upon physical collision with their environment. The array of interspaced obstacles provided an even inflow of medium and spore suspension, allowing for a balanced distribution of spores within the device, while giving plenty of opportunity for physical collisions.

Monitoring spore germination and asymbiotic hyphal growth

To demonstrate the functionality of the *AMF-SporeChip*, a germination assay was conducted with (i) *R. irregularis* MUCL 41833, (ii) *R. irregularis* MUCL 43194 and (iii) *R. intraradices* MUCL 49410. Since visual representation and a detailed description of spore germination within these species are scarce, illustrative timelapse images of the germination process have been provided herein (Fig. 2, Movies S1–S3†), acquired from the examination of a total of 600 spores. When comparing the different strains, we observed quite distinct differences in germination and hyphal growth patterns as well as spore shape, despite being closely related. While *R. irregularis* MUCL 41833 and *R. intraradices* MUCL 49410 have a nearly perfect circular spore shape in our study, *R. irregularis* MUCL 43194 spores came in various, elongated shapes (Fig. 2 and S1†). Generally, it was observed that *R. irregularis* MUCL 41833 germinated with a single hyphal branch, as observed in Fig. 2a, with occasionally up to 4 branches emerging from the germination site. Subsequent hyphal growth was found to be relatively linear and straight. In contrast, *R. irregularis* MUCL 43194 spores tended to branch more frequently at or shortly after the site of germination (*i.e.*, with typically 3–8 hyphae) as illustrated in Fig. 2b. Moreover, these asymbiotic hyphae possessed a curly and highly branched morphology. *R. intraradices* MUCL 49410 behaves similarly to *R. irregularis* MUCL 43194, with 3–6 hyphal branches emerging on average at or shortly after the germination site (Fig. 2c). Another interesting observation included an active discharge of phase-bright cellular contents

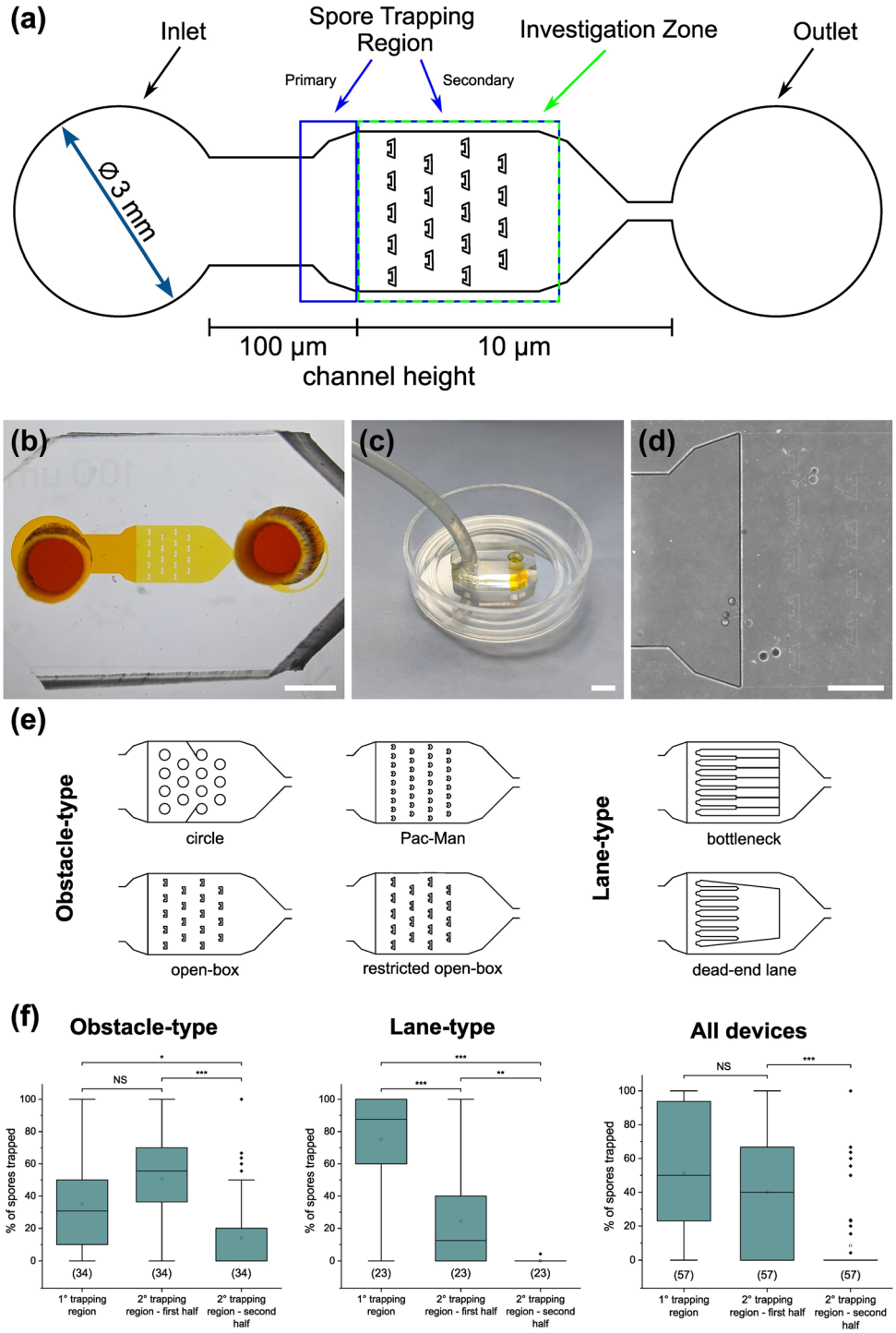

Fig. 1 Design of the *AMF-SporeChip*. (a) Two-dimensional schematic of the microfluidic device showing the dimensions and structure of the spore trapping region and investigation zone containing micron-sized obstacles. (b) Real life image of the device filled with 66 mM fluorescein solution to highlight the channels and the change in channel height. (c) The *AMF-SporeChip* fitted with tubing at the device inlet for the introduction of spores. The outer diameter of the Petri dish is 35 mm. (d) Brightfield image of the transition zone (microchannel height step-change) with trapped spores of *Rhizophagus irregularis* MUCL 41833. (e) Different geometries of the investigation zone of the *AMF-SporeChip*, including obstacle-type and lane-type structures. (f) Box-plots showing the percentage of spores trapped in each of the different trapping regions for lane-type and obstacle-type devices as well as all design types. Upper and lower whiskers represent the largest observation smaller or equal to the upper and lower percentile plus 1.5 × interquartile range, respectively. Squares indicate the means and the line the median. Data points beyond the whisker range (outliers) are plotted as diamonds. Significant differences according to one-way ANOVA are indicated with asterisks for p values <0.001 (***), <0.01(**) and <0.05 (*), as well as NS for no significant difference. The values in parentheses indicate the number of sample-points, *i.e.*, the number of microfluidic devices analysed. The total number of spores analysed was 260 for the lane-type devices and 473 for the obstacle-type devices. For the secondary trapping region – second half, the medians are 0 for lane-type devices as well as for "All devices", hence the number of values above 0 was insufficient to draw a box and were therefore categorised as outliers. Scale bars: (b) 2 mm; (c) 5 mm and (d) 500 µm.

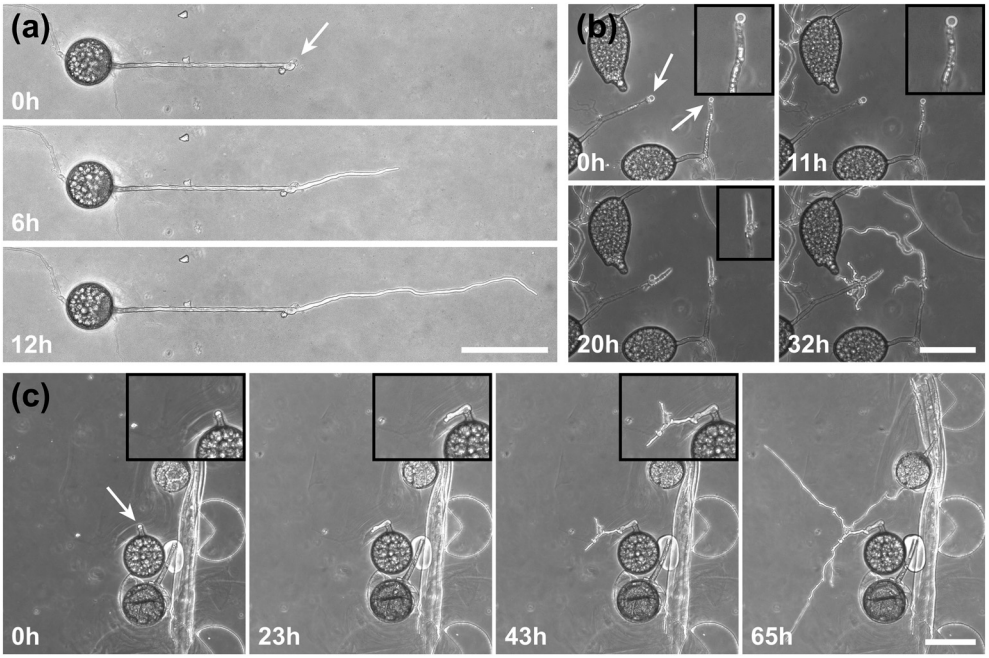

Fig. 2 AMF germination on chip. Time-series illustrating the germination process of (a) *Rhizophagus irregularis* MUCL 41833, (b) *Rhizophagus irregularis* MUCL 43194 and (c) *Rhizophagus intraradices* MUCL 49410. In (c), debris from the root-organ culture can be observed. White arrows indicate the germination site, with inset boxes in (b) and (c) illustrating an enlarged region of the germination event. Scale bars: 100 μm.

preceding germination (see Fig. 2b and Movie S2†). Occasionally, an internal collapse and emptying of the spore can be witnessed after a few days, after which the storage vesicles are ejected suddenly in one final load of cellular contents and nutrients into the attached hyphae (see Movie S4†). On several occasions, spore formation in asymbiotic hyphae, as reported by Dalpé *et al.*,[44] was observed (see Movie S5†).

For a quantitative analysis of growth dynamics on-chip in comparison to on-plate, hyphae of all three species were imaged and measured as described in the Experimental section. The results are illustrated in Fig. 3. For *R. irregularis* MUCL 41833, the on-chip measurements indicated a constant increase in spore germination. This is illustrated by the orange-coloured bar segments, which represent freshly germinated and short hyphae with a length of 0.1–0.4 mm, as well as a similarly constant growth of hyphae to lengths of 0.5–1.0 mm (green) and few hyphae to lengths of 1.1–3.0 mm (purple and yellow) and longer (>3 mm, blue). For *R. irregularis* MUCL 43194, a greater increase in the number of hyphae was observed over time on-chip, reaching a plateau after day 4, with few hyphae then growing longer. *R. intraradices* MUCL 49410 showed a constant increase in the number of hyphae over 7 days, similar to *R. irregularis* MUCL 43194, however with barely any hyphae growing further than 1.0 mm and only a few having lengths between 0.5–1.0 mm.

Growth on-plate generally yielded longer, fast-growing hyphae, reaching lengths of up to 20 mm, with slightly smaller total numbers of germination events, compared to on-chip. The trends illustrated by the stacked column charts within the first 7 days, which constitutes the main experimental phase used for all subsequent studies, however, are very much comparable and similar between on-chip and on-plate assay. Between day 7 and day 14, there was little growth and few germination events observed on-chip for *R. irregularis* MUCL 41833 (ratio of normalised count for day 14/7 = 1.082), while on-plate showed both elongating hyphae and new germinations (ratio of normalised count for day 14/7 = 1.263). For *R. irregularis* MUCL 43194, there were barely any further germination events observed, both on-chip and on-plate (on-chip ratio of normalised count for day 14/7 = 1.017; on-plate ratio of normalised count for day 14/7 = 1.047), with no further hyphal growth on-chip but further elongation on-plate. With *R. intraradices* MUCL 49410, there were numerous fresh germination events observed after 7 days, for both on-chip and on-plate experiments (on-chip ratio of normalised count for day 14/7 = 1.437; on-plate ratio of normalised count for day 14/7 = 1.549). Few hyphae were found to elongate further after 7 days on-plate, but not on-chip. The spore germination rates on-chip were found to be equally high between the three strains (no statistically significant differences), with means of 90.9% (*R. irregularis* MUCL 41833), 88.3% (*R. irregularis* MUCL 43194) and 92.5% (*R. intraradices* MUCL 49410). Germination rates on-plate could not be determined with this method. Due to the lack of confinement and thus focus, ungerminated germination sites could not be detected with certainty, highlighting the advantage of the *AMF-SporeChip*.

To highlight the versatility of the device, we modified the *AMF-SporeChip* to accommodate spores of *Gi. margarita*. Compared to the model organism *Rhizophagus* sp., as well as other AMF, *Gi. margarita* differs mainly in its macroscopic spore size. Further, a different anastomosis behaviour has

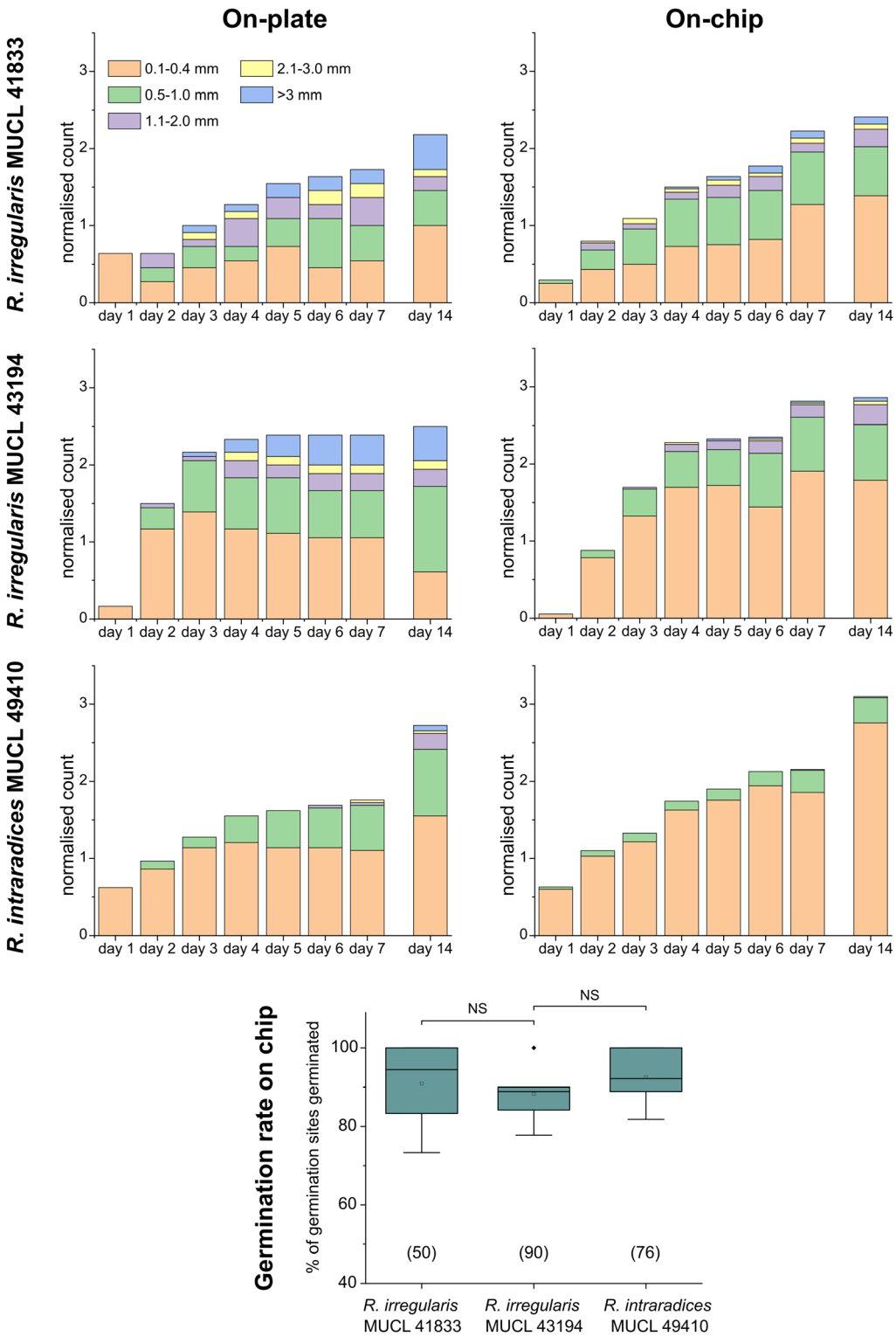

Fig. 3 Hyphal growth assay on-chip and on-plate. Stacked column charts showing the growth behaviour of *Rhizophagus irregularis* MUCL 41833, *Rhizophagus irregularis* MUCL 43194 and *Rhizophagus intraradices* MUCL 49410 in the *AMF-SporeChip* and on MSR(–) culture plates for comparison. Hyphal lengths were measured using ImageJ, normalised (number of germination sites was determined, and the absolute value of counts divided by the number of germination sites) and categorised in 5 length sections. For the hyphal growth behaviour, we counted sites where a germination within 14 days of inoculation occurred as germination sites. 6 devices with 40–60 germination sites in total per strain were used and 10–20 germination sites were found per plate. For calculation of the germination rates, we defined any site where usually a germination occurs from, *i.e.*, cut ends of hyphal remnants, as a germination site, which are indicated in parentheses below the boxes. Box-plot shows germination rates for all three AMF strains on-chip. Upper and lower whiskers represent the largest observation smaller or equal to the upper and lower percentile plus 1.5 × interquartile range, respectively. Squares indicate the means and the line the median. Data points beyond the whisker range (outliers) are plotted as diamonds. No significant differences between the results according to one-way ANOVA were found.

been documented.[15] By increasing the height of the microchannel in the spore trapping region from 100 to 350 μm, *Gi. margarita* spores were trapped successfully with subsequent germination and asymbiotic hyphal growth observed within the microchannels (Fig. 4). Upon encountering dead-end channels, the leading hypha bent and tracked the channel wall back in direction of the inlet, then branched in three different sites, *ca.* 350 μm, 720 μm and 1280 μm downstream from the hyphal tip. The hyphae then arrested growth and finally retracted the cytoplasm in a gradual manner, forming very pronounced septa (see Fig. 4 and Movie S6†).

"Stop-and-go" growth strategy prior to anastomosis formation

A highlight of the *AMF-SporeChip* involves the ability to observe fusion of hyphae to form a new cellular continuum, namely anastomosis. We witnessed both "tip-to-tip" and "tip-to-side" connections between hyphae originating from distinct spores, as well as from the same individuum. A representative depiction of anastomosis events observed within the *AMF-SporeChip* is shown in Fig. 5. The timelapse series presented show *R. irregularis* MUCL 43194 only; however, anastomosis events were also observed in *R. irregularis* MUCL 41833 and *R. intraradices* MUCL 49410. In Fig. 5a and b (and Movie S6†), a tip-to-tip anastomosis event can be observed. The hyphae approach each other from opposing directions with occasional arrestation of growth and readjustment of the growth direction. Fig. 5c quantifies the growth of both hyphae over a 21 h period. The left hypha approached the other hypha in 4 main growth phases. Both duration, as well as distance covered, decreased from the beginning to the end of data recording, with a growth rate of *ca.* 0.3 μm min^{-1} for the first two growth phases and 0.1 μm min^{-1} for the latter two. The growth phases were interrupted by arrestation of growth for *ca.* 3 h, then *ca.* 4 h and before the final growth phase <2 h. Meanwhile, the right hypha barely grows at all, covering a total distance of *ca.* 12 μm in the 21 h time period. In spite of having plenty of space to explore, and thus avoid one other, they specifically target the other hypha, indicating a clear signalling and searching prior to anastomosing (Fig. 5c and Movie S7†).

In Fig. 5d (and Movie S8†), a tip-to-tip anastomosis occurs in this instance, however, between a germination that is in progress and a hypha, rather than between two fully developed hyphae. The hypha approaching from the lower portion of the microscope image targets the end of an older hypha, which is just germinating, and fuses with the germination site. Following fusion, it can be clearly observed how a continuum is formed. Between timepoint 40 h and 80 h, cellular contents (phase-bright) are being pushed from the direction of the spore into the attached hypha. From this material, new branches are formed, concluding the process of unification. In Fig. 5e (and Movie S9†), a tip-to-side anastomosis can be observed. A hypha approaches from the bottom left corner of the image and after 4 h attaches laterally to the other hypha. Almost immediately, the

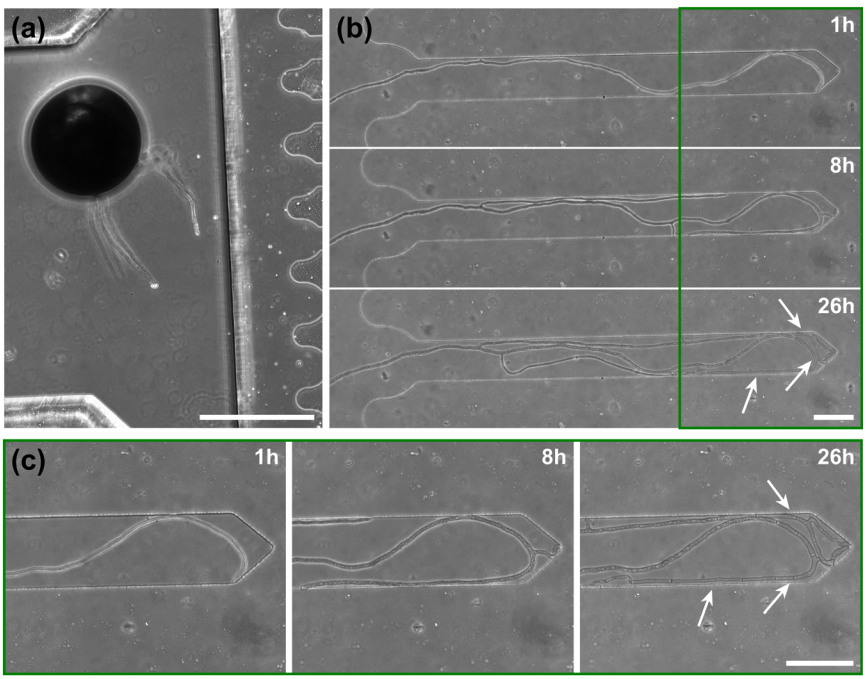

Fig. 4 *Gigaspora margarita* growing in a microfluidic device. Shown are (a) a spore of *Gi. margarita* trapped in the inlet and (b) a timelapse series of a *Gi. margarita* hypha growing into dead-end channels. When the hypha hits the wall, it bends, branches off in several positions and starts retracting cytoplasm from trapped tips. White arrows show examples of very pronounced septa formed in the retraction process. (c) Magnifications of the dead-end of the microchannel. White arrows indicate examples of septa. Image (a) was taken 2 days before the start of the timelapse series in (b). Scale bars: (a) 500 μm, (b and c) 100 μm.

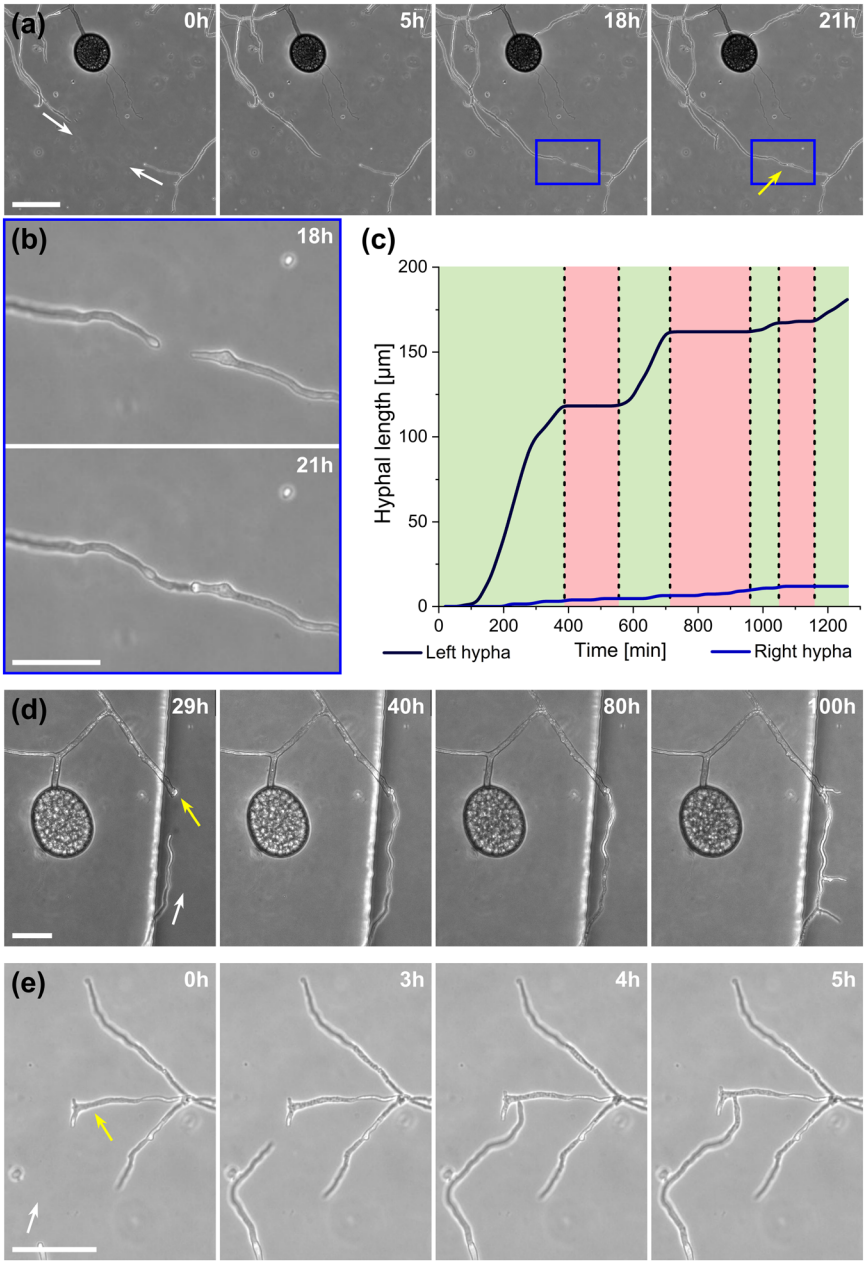

Fig. 5 Anastomosis formation of *Rhizophagus irregularis* MUCL 43194 in microfluidic device. (a) Two hyphae approaching one other and forming a tip-to-tip anastomosis. (b) An enlarged image of the moment just before contact and upon contact in (a). (c) Graph highlighting the growth of both hyphae before fusing, which illustrates the "stop-and-go" growth strategy of the left hypha, with the hypha on the right-hand side barely growing at all. (d) Another example of a tip-to-tip anastomosis event where, however, the hypha coming from the bottom of the image attaches to an older hypha, which is just about to germinate. Further, it can be observed how they from a continuum, with cellular contents (phase-bright) being pushed into the bottom hypha from the direction of the spore, with subsequent branching. (e) A tip-to-side anastomosis. Yellow arrows indicate the anastomosis site, white arrows indicate the growth direction of anastomosing hyphae. Scale bars: (a), (d) and (e) 50 μm; (b) 25 μm.

hyphae fuse and a cytoplasmic continuum is visible in the site of contact.

Hyphal behaviour upon encountering physical obstacles on the microscale

Inclusion of an array of obstacles within the investigation zone of the *AMF-SporeChip* afforded new insights into AMF spore hyphal growth dynamics. Specifically, the following was observed upon collision of *R. irregularis* MUCL 41833 hyphae with the restricted open-box obstacle (see Fig. 6 and Movie S10†). A hypha grew into the corner of the obstacle, *i.e.*, a dead-end, resulting in the hypha bending slightly and arresting growth. It then retracted the cytoplasm from the trapped tip and subsequently formed a septum *ca.* 40 μm downstream from the hyphal tip. The septa was then breached, and cytoplasm

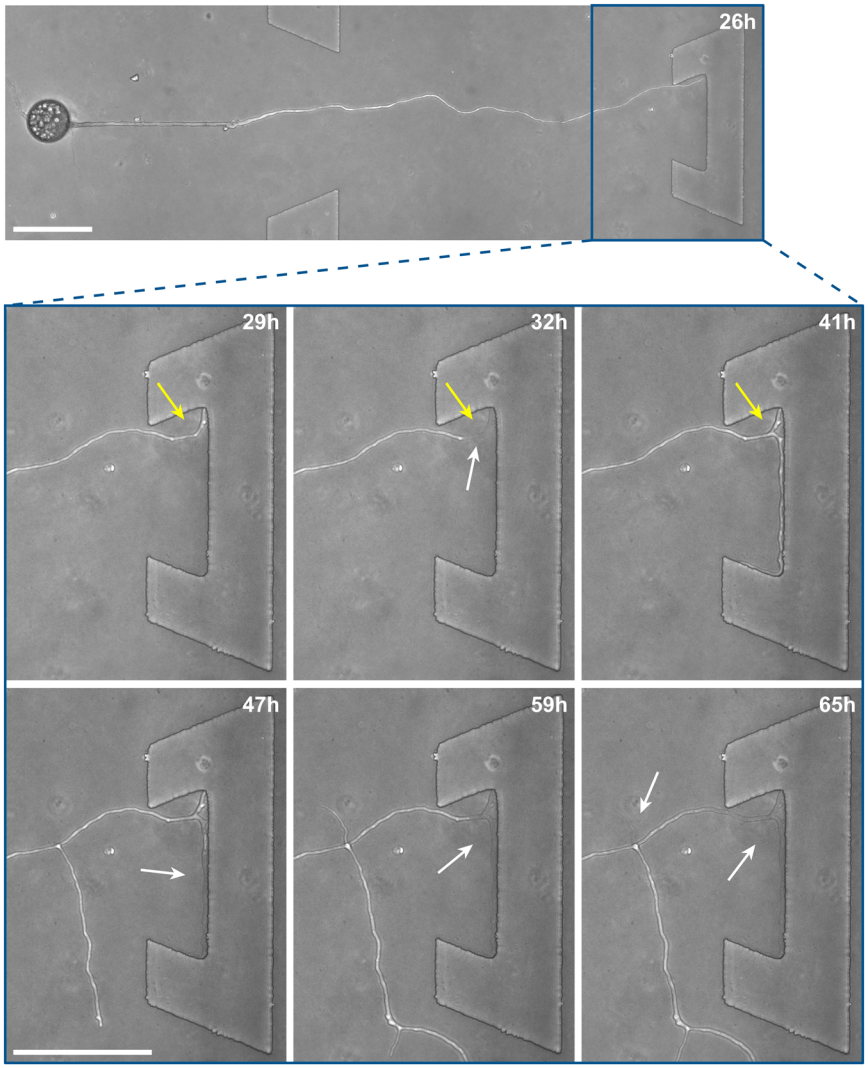

Fig. 6 Hyphal collision event in the *AMF-SporeChip*. Here, a time-series of images illustrates the dynamic behaviour of a *Rhizophagus irregularis* MUCL 41833 hypha upon interaction with an obstacle in the microfluidic device. Timepoint 0 h was defined as the point of spore germination. The hypha grows into the obstacle and becomes trapped, after which a series of dynamic, reversible cytoplasmic retraction and branching events occur in several positions at varying time points. Yellow arrows indicate the "reversible" cytoplasmic retraction, white arrows indicate "empty" hyphae following cytoplasmic retraction. Scale bars: 100 μm.

pumped back into the trapped hyphal tip followed by a new branch emerging shortly behind the tip. This new branch then grew towards the opposite corner of the obstacle and proceeded to track the edge of the obstacle for a few hours, with its tip now pointed towards the spore it originated from. It then stopped growing and retracted its cytoplasm with at least 2 visible septa formed downstream. A new hyphal branch emerged from a position outside the obstacle, followed by a second branch growing from the same branching point but into the opposite direction a few hours later. Eventually the fungus stopped growing to the left-hand side (with respect to initial growth direction) soon after and retracted further cytoplasm from this and the original, trapped branch and continued growing towards the right-hand side (with respect to initial growth direction), forming a bifurcation around hour 57 after the start of the experiment.

Interestingly, we observed several instances of reversible cytoplasmic retraction in both *R. irregularis* strains, not only with obstacles but also in open space. The number of septa formed upon retraction and septa breached upon reversal of the retraction varied (see Fig. 7a and Movie S11†), with up to 8 septa formed in a single retraction process and between 1 and 2 septa breached in the reversal phase. When the number of septa formed was higher than the number of septa breached, the retraction was not reversed all the way back to the hyphal tip and was hence incomplete. The retraction process varies not only in the number of septa formed/breached but also in the temporal dynamics (see Fig. 7b and c). Single retraction steps, *i.e.*, distance between tip and first septum or between septa, were found to be as fast as 30 min, however, can take up to 10 h. Similarly, some hyphae were observed to pause for up to 12 h between

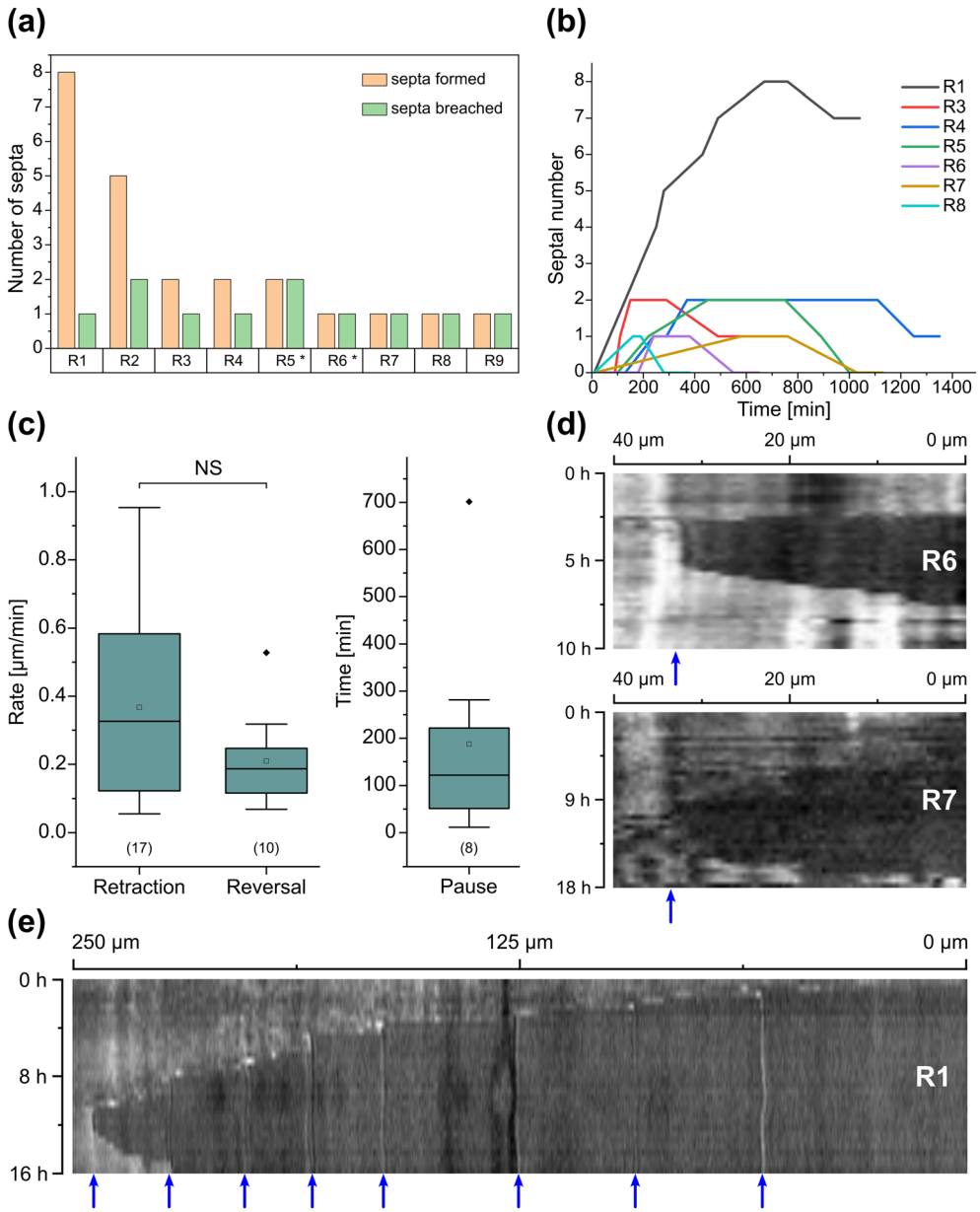

Fig. 7 Reversible cytoplasmic retraction in the *AMF-SporeChip*. (a) Column chart illustrating the number of septa formed and breached in the process of complete, as well as incomplete, reversible cytoplasmic retraction (R) upon interaction with obstacles (two instances, marked with asterisks; R5 and R6) as well as in open space (seven instances; R1–4 and R7–9). (b) Line graph showing temporal dynamics of the reversible retraction, highlighting timings for cytoplasmic retraction, pausing and reversal for the retraction events detailed in (a); for retraction R2 and R9, no sufficient temporally resolved data could be extracted. (c) Box-plots showing rates extracted from (b) for cytoplasmic retraction and reversal of the retraction as well as duration of pauses between retraction and reversal. Upper and lower whiskers represent the largest observation smaller or equal to the upper and lower percentile plus 1.5 × interquartile range, respectively. Squares indicate the means and the line the median. Data points beyond the whisker range (outliers) are plotted as diamonds. No significant difference between the rate of retraction and reversal according to one-way ANOVA was found, indicated as NS. The values in parentheses indicate the number of sample-points, *i.e.*, the number of events analysed. (d) Kymograph analysis of retraction R6 and R7 and (e) kymograph analysis of retraction R1. Blue arrows indicate septa. All retraction events were found with *Rhizophagus irregularis* MUCL 41833, except R3 and R9, which were found with *Rhizophagus irregularis* MUCL 43194.

retraction and reversal, while some reverse the process within minutes. The reversal was slightly less variable, with timings between 1 and 3 h. Retraction and reversal rates were calculated using the distance between two septa or tip and first septum, which was on average 26.3 ± 11.8 µm. The retraction (mean = 0.4 ± 0.3 µm min^{-1}) and reversal rates (mean = 0.2 ± 0.1 µm min^{-1}) were not found to be significantly different, however, a stronger variation in the rate of retraction can be observed. The kymographs in Fig. 7d and e visualise the entire retraction process in further detail for retractions R1, R6 and R7. It shows a strong asymmetry between retraction and reversal rate with a much

faster retraction and a slower reversal in R6, contrasted by a very slow retraction and relatively fast reversal for R7. In the kymograph for R1, it can be observed how the first retraction steps occur within a very short time frame, despite covering relatively long distances, while the last steps of the retraction with only little distance to cover take much longer (which is the case for the reversal in the last septum).

Besides this novel observation, further observations were made, described before in studies with other fungi, such as "hit-and-split" (see Movie S12†), tracking (*e.g.*, in Fig. 6 and Movie S10†) as well as numerous instances of irreversible cytoplasmic retraction in both obstacle and open space (*e.g.*, in Fig. 6 and Movie S11†). Growth arrest in hyphae was often found to coincide with cytoplasmic retraction within a few hours. However, in a few cases we found hyphae to freeze for long periods of time (tens of hours) before finally retracting their cytoplasm (see Movie S13†) or hitting an obstacle or a wall but continuing to grow and thus bending and gradually pushing itself away from the obstacle as if not recognising it (see Movie S14†).

To further highlight certain sub-cellular structures and characterise the nature of the hyphae observed in the cytoplasmic retraction, we employed two different fluorescent dyes, namely calcofluor white (CFW) and FM4-64 for end point staining. In Fig. 8a, all hyphae are visible in the phase contrast microscopy image, regardless of their developmental stage, however with differences observable, *i.e.*, "normal" phase-bright hyphae and "empty" phase-dark hyphae, the latter of which is akin to what is observed after cytoplasmic retraction. Staining with the chitin specific dye, calcofluor white, reveals all hyphae observed in the phase contrast image (Fig. 8b). In Fig. 8c only some hyphae are visible; here, the dye FM4-64 is employed, which stains lipid bilayers, *i.e.*, membranes and organelles. Thus, only viable hyphae that contain all cellular contents remain detectable. Cytoplasmic retraction is followed by sequential formation of septa, which separate the cytoplasm-filled portion of a hypha from the empty portion. These septa are visible in phase-dark hyphae in the phase contrast image and are particularly pronounced in the CFW staining.

Discussion

The *AMF-SporeChip* provides high-resolution dynamic imaging of AMF in defined environments

Here, we present the first microfluidic device of its kind, namely the *AMF-SporeChip*, designed to accommodate AMF spores for studying germination and the dynamic behaviour of asymbiotic hyphal growth at the cellular level. The device was specifically designed to trap spores of *Rhizophagus* and later adapted for *Gi. margarita*. The trapping relied on two main aspects, the first being simply a difference in channel height, which kept about 50% of *Rhizophagus* spores out of the investigation zone, while allowing the much smaller hyphae to grow in. Secondly, the high flexibility of PDMS allowed *ca.* 40% of the *Rhizophagus* spore population to be trapped in the first half of the secondary trapping region. This trait of PDMS is actively utilised for cell trapping in microfluidics, mainly with yeast cells,[44–46] but has also been used to measure force exerted by fungal-like Oomycete hyphal tips.[47] Here, the two trapping mechanisms facilitate a reliable introduction of spores into and even distribution within the devices. The application of microfluidic technologies for the study of yeast has received plenty of attention in the last two decades,[21] yet for other types of fungi, this technique is still very new. Indeed, its utility has been demonstrated only in a handful of studies,[24,48,49] which focussed mainly on examining the space-searching behaviour of filamentous fungi or interactions between fungi and other microorganisms,[29,33,35] but has never before considered AMF spore germination or asymbiotic hyphal growth.

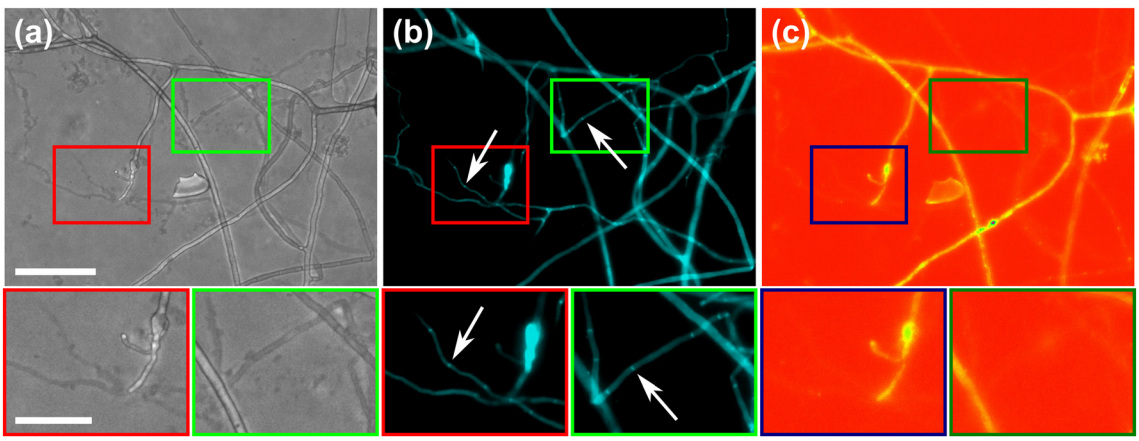

Fig. 8 Differential staining of vital and empty hyphae. The images displayed refer to the same region of interest within the *AMF-SporeChip* and represent: (a) phase contrast, (b) DAPI and (c) TRITC channels. The fluorescent dyes used in this study include calcofluor white (CFW), which stains chitin in the cell walls and FM4-64, staining lipid bilayers. White arrows indicate two exemplary hyphae which were emptied, with pronounced septa as artefacts of gradual retraction of cytoplasm. The images were edited using ImageJ/Fiji. The lookup tables "cyan" (b) and "spectrum" (c) were applied to improve the visibility of fluorescence intensity. Scale bar: 100 μm, 50 μm in zoomed-in images.

Importantly, our devices featured obstacles within the investigation zone to mimic (micro) structures (*i.e.*, soil microaggregates) in their natural habitat by blocking their growth path and provoking physical collisions. The various designs provided hyphae with differing opportunities to interact with or escape from an obstacle; the "restricted open-box" or the "dead-end lane" designs forced hyphae to arrest growth or change direction entirely, for instance. For AMF asymbiotic hyphae, this behaviour has never been studied before. Investigating how the fungal mycelium adapts to the physical conditions in soil is important for understanding a fungus' lifestyle and eventually utilising this knowledge for potential applications in agriculture and horticulture/restoration as well as for the preservation of natural ecosystems.

Microfluidics-assisted imaging yields detailed visuals of spore germination in real-time

Germination of AMF spores has been described in the literature,[51] however, high-resolution visual material is scarcely available. To demonstrate the strength of the microfluidic approach and as proof-of-concept, we captured high resolution timelapse videos of spores of the three *Rhizophagus* strains studied, as well as with *Gi. margarita*.

Interestingly, distinct germination and branching patterns were observed between *R. irregularis* MUCL 41833 and MUCL 43194 (despite being two strains of the same species, and besides differences in shape and size), which suggest different exploration strategies. While *R. irregularis* MUCL 41833 germinated with 1–4 rather straight hyphae from the germination site, *R. irregularis* MUCL 43194 germinated with between 3–8 curly hyphae, which readily branched again shortly after the germination. Measuring hyphal elongation every 24 h for a week further revealed that *R. irregularis* MUCL 41833 has a growth pattern which is relatively balanced between new germination and hyphal elongation, whereas *R. irregularis* MUCL 43194 tended to germinate a lot more over the first 3 days and then resulted in elongation of some of these hyphae, corroborating the visually observed growth behaviour in both strains. It appears this strain first establishes a base around the spore and then starts exploring with single runner hyphae, while *R. irregularis* MUCL 41833 does not hesitate and starts exploring straight away with runner hyphae shooting randomly from the spore. The physiological stage (*i.e.*, spore age) was not taken into consideration. For both strains, hyphal elongation proceeded after day 7 but rarely were any new germinations observed. *R. intraradices* MUCL 49410 behaves in a similar manner to *R. irregularis* MUCL 43194, with typically 3–6 curly and branched hyphae emerging from one germination site, which, however, barely ever extended beyond 1 mm. Fresh germination events on the other hand continued to occur numerously even beyond day 7 until the end of the experiment.

For all three strains studied, the on-plate results followed closely the findings from the on-chip experiments, with the exception of increased hyphal elongation on-plate. This difference in growth is a pre-described observation, which occurs in microfluidic devices and could be explained by two observations: (i) the microchannels are saturated with culture medium, *i.e.*, the fungi are submersed in liquid, while on-plate they grow in an environment that has a solid phytagel base, with a liquid film on top as well as direct contact with air; (ii) the hyphae are physically confined inside microchannels, which has been suspected to influence hyphal growth.[52] Filamentous fungi are known to possess mechanosensory properties[53] allowing them to sense the confinement and adapt their growth accordingly. This sensing happens both on a mechanical level, upon direct contact with the wall or the obstacle, as well as chemical level, where the fungus recognises the surface functionalisation.[54] Overall, we can conclude from our results, however, that the germination and growth behaviour in the *Rhizophagus* strains is very much comparable between on-chip and on-plate and hence our microdevices are suitable to study these fungi. Further, the devices were modified to accommodate the much bigger spores of *Gi. margarita* and it was demonstrated that they, too, can germinate in the microdevice, illustrating the flexibility of our platform.

Anastomosis formation involves directed growth with readjustments in a "stop-and-go" manner

Another phenomenon implicating hyphal space searching strategies is anastomosis formation. Filamentous fungi are able to connect their hyphae with another individuum of the same strain or in a "self–self" manner (*i.e.*, hyphae from the same individuum).[55,56] Even interspecies anastomoses have been reported.[57] Fungi anastomose to interconnect and expand their mycelial network for exploring and foraging, to exchange nutrients[58] and genetic material,[59] to heal damages in the hyphal network[15] or even to form traps to capture nematodes.[60] Here, anastomoses were observed between different individuals of the same strain as well as self–self, and formed in a tip-to-tip or tip-to-side manner. Our high-resolution imaging approach, which affords a relatively large confined observation area, provided real-time videos of the entire anastomosis process in asymbiotic hyphae. This allowed us to image hyphal approach from a wide angle through to complete fusion, extending experimental opportunities detailed by de la Providencia *et al.*[15] and Voets *et al.*[61] for intraradical hyphae. As such, the *AMF-SporeChip* revealed how two hyphae hesitantly approached one other from opposing directions in a stop-and-go manner, occasionally halting to readjust growth direction. It is clear that these hyphae actively target each other since there is plenty of space for avoidance, which suggests an underlying signalling and decision-making that leads to tropism for one other. This was further corroborated by the occasional observation of hyphal contact that did not lead to successful anastomosis, indicated by cytoplasmic retraction and septation as earlier described by Giovannetti *et al.*[62] In certain filamentous fungi, it has been reported that there are

even specialised hyphae for fusion.[63,64] Large scale follow-up studies are now needed to explore this further.

Dynamic hyphal reactions involving reversible cytoplasmic retraction in obstacle-containing environments

The obstacles featured in our devices were designed to trigger collision events, which we hypothesised would provoke a response in AMF asymbiotic hyphae akin to that described for AMF extraradical hyphae[65] as well as for other filamentous fungi.[50,65,66] Expected phenotypes involved apical and lateral branching, tracking or nestling, as well as hit-and-split events.[67] Several instances of lateral branching were observed, occasional tracking of obstacle shapes, as well as one case of hit-and-split, though no true apical branching was found. Both irreversible and reversible cytoplasmic retraction were found with obstacles as well as in open space. Furthermore, collisions with obstacles did not always result in cytoplasmic retraction, at least not immediately, and instead hyphal growth ensued and resulted in hyphae gradually pushing themselves away from an obstacle as if they did not recognise, or tried to force their way through, the obstacle. Occasionally, hyphae froze mid-growth and remain unchanged for days without cytoplasmic retraction, highlighting a high overall versatility and breadth of their growth mechanisms.

As a new finding in this study, we identified a reversible cytoplasmic retraction, which involved withdrawal of cytoplasm, septa formation, breaching of septa and reintroduction of cytoplasm into previously emptied hyphae. Generally, it was observed that hyphae try to grow around an obstacle upon encountering it, tracking its edge to "escape" the obstacle. If the obstacle proves to be impassable, such as in dead-end corners, the fungus responds by branching off into another direction. As AMF are obligate symbionts (*i.e.*, do not possess saprotrophic capabilities) and their sole focus is to find a suitable host as fast as possible,[68] hyphae and spores have to be highly economical with their resources in the explorative asymbiotic state. Therefore, when the original growth path is blocked or appears unfavourable, they retract cytoplasm containing all cellular contents from the hyphal tip in order to redistribute it to another branch of the hyphal network; this retraction is a common observation in filamentous fungi in general,[69] as well as in AMF,[70,71] usually as a defence mechanism to keep the mycelial network from global compromisation.[72] The novelty of our finding, however, is that this process can be reversible in *R. irregularis* MUCL 41833 and MUCL 43194. The septa, which are formed to segregate empty compartments within a hypha from those that are filled, can be breached and cellular contents reintroduced into the emptied segments. Opening and closing of septa in septate fungi is a well-studied and common process. In Ascomycetes, for example, a so-called Woronin body functions as a plug for septa pores allowing for a controlled, selective permeability through these septa.[73] In non-septate fungi like AMF, where septation is of a primarily defensive nature, septal opening and closing has not been thoroughly described to date. Lee[74] proposed the removal of septa to control the expansion of cytoplasmic contents into new hyphal area in *Rhizophagus*. It can be assumed that septa are broken down entirely, as well as being newly formed, when compartmentalisation is needed. The observed reversible cytoplasmic retraction with septation, together with branching, makes hyphal exploration a highly dynamic process.

The repopulation of emptied hyphae might be an attempt to re-explore avenues to adapt to a changing environment, again with minimised resource requirements. Which signal or stimulus induces the retraction/repopulation here is unknown. Interestingly, we found that the number of formed septa was not always matched with the same number of septa breached, *i.e.*, the reversal of the retraction did not always occur all the way back to the hyphal tip, meaning the retraction can be reversed completely (*i.e.*, number of septa formed = number of septa breached) or incompletely (*i.e.*, number of septa formed > number of septa breached). The temporal dynamics of the retraction process were found to be most variable, with timings for retraction, reversal and pauses between retraction and reversal events fluctuating within a range of hours. No significant difference could be found for the retraction and reversal rates, which, however, does not mean retraction and reversal rates within a particular retraction event are always symmetrical. Furthermore, there was found to be less variation in reversal rates *cf.* retraction rates. To consolidate these observations and also to explore the influence of obstacles on the frequency, rates as well as symmetry of the retraction process, future focussed studies need to be conducted to obtain a higher sample size by, for example, implementing higher obstacle or spore densities in the devices as well as attempting to increase microscopy throughput for parallelised timelapse imaging. New preliminary insights into the dynamic behaviour of AMF at the cellular level, including identification of a reversible cytoplasmic retraction, were made possible using our high-resolution, real-time microfluidic approach.

To further characterise the reversible retraction of cytoplasm observed during hyphal space searching, we introduced the fluorescent dyes FM4-64[75–77] and calcofluor white[78–80] into the *AMF-SporeChip* to stain hyphae. Both dyes stained the fungal hyphae successfully and confirmed the identity of emptied hyphae. As expected, the chitin-specific calcofluor white stained every hypha, while the lipid bilayer-specific FM4-64 only stained certain hyphae, which usually appeared phase-dark under phase contrast, corroborating the finding that hyphae were emptied of their cytoplasmic content. In these empty hyphal "shells", only a very faint signal at 544 nm was visible; however, due to a slight autofluorescence of the studied strains it cannot be known with certainty whether the cell membrane remains behind after retraction of the cytoplasm, or rather is removed completely or decays shortly after the event. Implementation of fluorescent dyes such as these, especially FM4-64, for live-cell imaging of AMF hyphae in combination with our microdevices will help to characterise the dynamic retraction process in further detail, as well as aid examination of AMF hyphae for a potential Spitzenkörper.

Conclusions

We have presented the first microfluidic device for studying AMF germination, asymbiotic hyphal development, anastomosis formation and space searching at the cellular level, which has provided new insights into AMF hyphal growth dynamics and revealed an intricate mechanism of space searching involving reversible cytoplasmic retraction, branching and directional changes. In the future, it is envisaged that the *AMF-SporeChip* could be modified easily to investigate several new frontiers in AMF research. One example includes modifying the design to accommodate two different strains of AMF simultaneously for the study of anastomosis phenotypes in a systematic manner. Further, our device could equally be used as a suitable platform to gain a deeper understanding of septa, as well as whether asymbiotic AMF hyphae possess a Spitzenkörper. To study metabolites involved in signalling, microfluidics could offer the opportunity to collect the fluidic volume for downstream metabolomics analyses, following visual examinations of these events. Our design is not only limited to AMF, as other fungal spores can be introduced into the *AMF-SporeChip* in a similar manner. Moreover, gradients of chemicals or nutrients can be implemented for studying foraging and signalling in soil exploration. The further development of our device could be also utilised for experiments on AMF interactions with bacteria, *e.g.*, phosphate solubilising bacteria, which have been reported to be important for phosphate uptake in AMF,[81] suggesting a tripartite symbiosis between plant, fungus and bacteria. To study the AMF symbiosis with their host roots in more detail, a device built from a combination of the *AMF-SporeChip* and the *RootChip*[82] could be of assistance.

Data availability

All relevant data are available from the corresponding author upon request.

Author contributions

The idea for the *AMF-SporeChip* and study was conceived by C. E. S., F. R. designed and fabricated the microfluidic device, and performed the experiments, the microscopy imaging and the data analysis. M. C. prepared the spore samples, as well as advice and training with regard to setting up AMF *in vitro* cultures. C. E. S. supervised this study, whereas S. D. and M. H. provided valuable feedback to the experimental work. F. R. and C. E. S. took the lead in writing the manuscript with contributions from all other authors. All authors read and approved the final version of the manuscript.

Conflicts of interest

The are no conflicts of interest to declare.

Acknowledgements

We acknowledge financial support from the Department of Bioengineering at Imperial College London, as well as the Swiss National Science Foundation in the form of an Ambizione Career Grant (PZ00P2_168005) to C. E. S. We thank Dr Emily Masters-Clark for informative scientific discussions.

References

1 P. Bonfante and A. Genre, *Nat. Commun.*, 2010, **1**, 48.
2 M. Cosme, I. Fernandez, M. G. A. van der Heijden and C. M. J. Pieterse, *Trends Plant Sci.*, 2018, **23**, 577–587.
3 M. G. A. van der Heijden, F. M. Martin, M. A. Selosse and I. R. Sanders, *New Phytol.*, 2015, **205**, 1406–1423.
4 R. M. Miller, J. D. Jastrow and D. R. Reinhardt, *Oecologia*, 1995, **103**, 17–23.
5 S. E. Smith and D. Read, in *Mycorrhizal Symbiosis (Third Edition)*, ed. S. E. Smith and D. Read, Academic Press, London, UK, 2008, pp. 145–188, DOI: **10.1016/B978-012370526-6.50007-6**.
6 I. Jakobsen and L. Rosendahl, *New Phytol.*, 1990, **115**, 77–83.
7 J. Shi, X. Wang and E. Wang, *Annu. Rev. Plant Biol.*, 2023, **74**, 569–607.
8 M. G. A. van der Heijden, R. D. Bardgett and N. M. van Straalen, *Ecol. Lett.*, 2008, **11**, 296–310.
9 S. W. Simard, K. J. Beiler, M. A. Bingham, J. R. Deslippe, L. J. Philip and F. P. Teste, *Fungal Biol. Rev.*, 2012, **26**, 39–60.
10 D. E. Prado-Tarango, R. Mata-González, M. Hovland and R. P. Schreiner, *Rangel. Ecol. Manag.*, 2021, **79**, 87–90.
11 A. Berruti, E. Lumini and V. Bianciotto, *Symbiosis*, 2016, **72**, 73–80.
12 E. Verbruggen, M. G. van der Heijden, M. C. Rillig and E. T. Kiers, *New Phytol.*, 2013, **197**, 1104–1109.
13 X. Zhu, K. Wang, H. Yan, C. Liu, X. Zhu and B. Chen, *Environ. Sci. Technol.*, 2022, **56**, 711–731.
14 M. Ijdo, S. Cranenbrouck and S. Declerck, *Mycorrhiza*, 2011, **21**, 1–16.
15 I. E. de la Providencia, F. A. de Souza, F. Fernandez, N. S. Delmas and S. Declerck, *New Phytol.*, 2005, **165**, 261–271.
16 I. E. De La Providencia, F. Fernández and S. Declerck, *FEMS Microbiol. Lett.*, 2007, **268**, 120–125.
17 M. Giovannetti, L. Ayio, C. Sbrana and A. Silvia Citernesi, *New Phytol.*, 1993, **123**, 115–122.
18 M. Giovannetti, P. Fortuna, A. S. Citernesi, S. Morini and M. P. Nuti, *New Phytol.*, 2001, **151**, 717–724.
19 M. Giovannetti, C. Sbrana, P. Strani, M. Agnolucci, V. Rinaudo and L. Avio, *Appl. Environ. Microbiol.*, 2003, **69**, 616–624.
20 D. Croll, M. Giovannetti, A. M. Koch, C. Sbrana, M. Ehinger, P. J. Lammers and I. R. Sanders, *New Phytol.*, 2009, **181**, 924–937.
21 F. Richter, S. Bindschedler, M. Calonne-Salmon, S. Declerck, P. Junier and C. E. Stanley, *FEMS Microbiol. Rev.*, 2022, fuac039, DOI: **10.1093/femsre/fuac039**.

22 M. Held, C. Edwards and D. V. Nicolau, *J. Phys.: Conf. Ser.*, 2009, **178**, 012005.
23 M. Held, A. P. Lee, C. Edwards and D. V. Nicolau, *Microelectron. Eng.*, 2010, **87**, 786–789.
24 M. Held, C. Edwards and D. V. Nicolau, *Fungal Biol.*, 2011, **115**, 493–505.
25 M. Held, M. Binz, C. Edwards and D. Nicolau, *Proc. SPIE*, 2009, 7182.
26 D. D. Thomson, S. Wehmeier, F. J. Byfield, P. A. Janmey, D. Caballero-Lima, A. Crossley and A. C. Brand, *Cell. Microbiol.*, 2015, **17**, 342–354.
27 C. Puerner, N. Kukhaleishvili, D. Thomson, S. Schaub, X. Noblin, A. Seminara, M. Bassilana and R. A. Arkowitz, *BMC Biol.*, 2020, **18**, 122.
28 E. Couttenier, S. Bachellier-Bassi, C. d'Enfert and C. Villard, *Lab Chip*, 2022, **22**, 3898–3909.
29 C. E. Stanley, M. Stockli, D. van Swaay, J. Sabotic, P. T. Kallio, M. Kunzler, A. J. deMello and M. Aebi, *Integr. Biol.*, 2014, **6**, 935–945.
30 M. Stockli, B. I. Morinaka, G. Lackner, A. Kombrink, R. Sieber, C. Margot, C. E. Stanley, A. J. deMello, J. Piel and M. Kunzler, *Mol. Microbiol.*, 2019, **112**, 605–619.
31 L. J. Millet, J. Aufrecht, J. Labbe, J. Uehling, R. Vilgalys, M. L. Estes, C. Miquel Guennoc, A. Deveau, S. Olsson, G. Bonito, M. J. Doktycz and S. T. Retterer, *Fungal Biol. Biotechnol.*, 2019, **6**, 1.
32 J. K. Uehling, M. R. Entler, H. R. Meredith, L. J. Millet, C. M. Timm, J. A. Aufrecht, G. M. Bonito, N. L. Engle, J. L. Labbe, M. J. Doktycz, S. T. Retterer, J. W. Spatafora, J. E. Stajich, T. J. Tschaplinski and R. J. Vilgalys, *Front. Microbiol.*, 2019, **10**, 2163.
33 S. S. Schmieder, C. E. Stanley, A. Rzepiela, D. van Swaay, J. Sabotic, S. F. Norrelykke, A. J. deMello, M. Aebi and M. Kunzler, *Curr. Biol.*, 2019, **29**, 217–228.e4.
34 N. Ghanem, C. E. Stanley, H. Harms, A. Chatzinotas and L. Y. Wick, *Environ. Sci. Technol.*, 2019, **53**, 11755–11763.
35 A. Gimeno, C. E. Stanley, Z. Ngamenie, M. H. Hsung, F. Walder, S. S. Schmieder, S. Bindschedler, P. Junier, B. Keller and S. Vogelgsang, *Commun. Biol.*, 2021, **4**, 262.
36 K. Srisom, P. Tittabutr, N. Teaumroong, Y. Lapwong, R. Phatthanakun, S. Sirivisoot and P. Kuntanawat, *Mycorrhiza*, 2020, **30**, 789–796.
37 P. M. Mafla-Endara, C. Arellano-Caicedo, K. Aleklett, M. Pucetaite, P. Ohlsson and E. C. Hammer, *Commun. Biol.*, 2021, **4**, 889.
38 C. Baranger, I. Pezron, L. Lins, M. Deleu, A. Le Goff and A. Fayeulle, *Sci. Total Environ.*, 2021, **784**, 147151.
39 S. Declerck, D. Strullu and C. Plenchette, *Mycologia*, 1998, **90**, 579–585.
40 S. Cranenbrouck, L. Voets, C. Bivort, L. Renard, D.-G. Strullu and S. Declerck, in *In Vitro Culture of Mycorrhizas*, ed. S. Declerck, J. A. Fortin and D.-G. Strullu, Springer Berlin Heidelberg, Berlin Heidelberg, Germany, 2005, pp. 341–375, DOI: **10.1007/3-540-27331-X_18**.
41 M. Köfferlein, *KLayout—high performance layout viewer and editor, v.0.27.25*, Munich, Germany, 2006, **https://www.klayout.de/**.
42 J. Schindelin, I. Arganda-Carreras, E. Frise, V. Kaynig, M. Longair, T. Pietzsch, S. Preibisch, C. Rueden, S. Saalfeld and B. Schmid, *Nat. Methods*, 2012, **9**, 676–682.
43 S. S. Lee, I. Avalos Vizcarra, D. H. Huberts, L. P. Lee and M. Heinemann, *Proc. Natl. Acad. Sci. U. S. A.*, 2012, **109**, 4916–4920.
44 Y. Dalpé, F. A. de Souza and S. Declerck, in *In Vitro Culture of Mycorrhizas*, ed. S. Declerck, J. A. Fortin and D.-G. Strullu, Springer Berlin Heidelberg, Berlin, Heidelberg, 2005, pp. 49–71, DOI: **10.1007/3-540-27331-X_4**.
45 A. Groisman, C. Lobo, H. Cho, J. K. Campbell, Y. S. Dufour, A. M. Stevens and A. Levchenko, *Nat. Methods*, 2005, **2**, 685–689.
46 P. J. Lee, N. C. Helman, W. A. Lim and P. J. Hung, *BioTechniques*, 2008, **44**, 91–95.
47 Y. Zhang, C. Luo, K. Zou, Z. Xie, O. Brandman, Q. Ouyang and H. Li, *PLoS One*, 2012, **7**, e48275.
48 Y. Sun, A. Tayagui, A. Garrill and V. Nock, *Lab Chip*, 2020, **20**, 4141–4151.
49 S. Fukuda, R. Yamamoto, N. Yanagisawa, N. Takaya, Y. Sato, M. Riquelme and N. Takeshita, *mBio*, 2021, **12**, e03196-20.
50 A. Hopke, A. Mela, F. Ellett, D. Carter-House, J. F. Pena, J. E. Stajich, S. Altamirano, B. Lovett, M. Egan, S. Kale, I. Kronholm, P. Guerette, E. Szewczyk, K. McCluskey, D. Breslauer, H. Shah, B. R. Coad, M. Momany and D. Irimia, *PLoS One*, 2021, **16**, e0257823.
51 T. Souza, *Handbook of arbuscular mycorrhizal fungi*, Springer, Cham, Switzerland, 2015.
52 C. Baranger, A. Fayeulle and A. Le Goff, *R. Soc. Open Sci.*, 2020, **7**, 191535.
53 C. A. Kumamoto, *Nat. Rev. Microbiol.*, 2008, **6**, 667–673.
54 M. Held, D. L. Farkas, C. Edwards, D. V. Nicolau, R. C. Leif and D. V. Nicolau, *Proc. SPIE*, 2011, **7902**, 79020S-1.
55 C. B. D. Novais, A. Pepe, J. O. Siqueira, M. Giovannetti and C. Sbrana, *Sci. Agric.*, 2017, **74**, 411–416.
56 N. L. Glass, D. J. Jacobson and P. K. T. Shiu, *Annu. Rev. Genet.*, 2000, **34**, 165–186.
57 M. G. Roca, L. C. Davide, L. M. C. Davide, M. C. Mendes-Costa, R. F. Schwan and A. E. Wheals, *Mycol. Res.*, 2004, **108**, 1320–1326.
58 A. Fleißner, A. R. Simonin and N. L. Glass, in *Cell Fusion: Overviews and Methods*, ed. E. H. Chen, Humana Press, Totowa, NJ, 2008, pp. 21–38, DOI: **10.1007/978-1-59745-250-2_2**.
59 T. L. Friesen, E. H. Stukenbrock, Z. Liu, S. Meinhardt, H. Ling, J. D. Faris, J. B. Rasmussen, P. S. Solomon, B. A. McDonald and R. P. Oliver, *Nat. Genet.*, 2006, **38**, 953–956.
60 H. Haj Hammadeh, A. Serrano, V. Wernet, N. Stomberg, D. Hellmeier, M. Weichert, U. Brandt, B. Sieg, K. Kanofsky, R. Hehl, R. Fischer and A. Fleißner, *Proc. Natl. Acad. Sci. U. S. A.*, 2022, **119**, e2112518119.
61 L. Voets, I. E. De La Providencia and S. Declerck, *New Phytol.*, 2006, **172**, 185–188.
62 M. Giovannetti, D. Azzolini and A. S. Citernesi, *Appl. Environ. Microbiol.*, 1999, **65**, 5571–5575.
63 P. M. McCabe, M. P. Gallagher and J. W. Deacon, *Mycol. Res.*, 1999, **103**, 487–490.

64 N. D. Read, A. Lichius, J.-Y. Shoji and A. B. Goryachev, *Curr. Opin. Microbiol.*, 2009, **12**, 608–615.
65 E. C. Hammer, C. Arellano-Caicedo, P. M. Mafla-Endara, E. T. Kiers, T. Shimizu, P. Ohlsson and K. Aleklett, *Fungal Ecol.*, 2024, **67**, 101302.
66 K. Aleklett, P. Ohlsson, M. Bengtsson and E. C. Hammer, *ISME J.*, 2021, **15**, 1782–1793.
67 M. Held, O. Kaspar, C. Edwards and D. V. Nicolau, *Proc. Natl. Acad. Sci. U. S. A.*, 2019, **116**, 13543–13552.
68 S. E. Smith and D. J. Read, *Mycorrhizal Symbiosis*, Elsevier Science, Amsterdam, Netherlands, 2010.
69 A. P. Martínez-Camacho, M. O. Cortez-Rocha, M. M. Castillo-Ortega, A. Burgos-Hernández, J. M. Ezquerra-Brauer and M. Plascencia-Jatomea, *Polym. Int.*, 2011, **60**, 1663–1669.
70 V. Kokkoris, F. Stefani, Y. Dalpé, J. Dettman and N. Corradi, *Trends Plant Sci.*, 2020, **25**, 765–778.
71 B. Bago, C. Azcón-Aguilar, A. Goulet and Y. Piché, *New Phytol.*, 1998, **139**, 375–388.
72 C. Logi, C. Sbrana and M. Giovannetti, *Appl. Environ. Microbiol.*, 1998, **64**, 3473–3479.
73 R.-J. Bleichrodt, M. Hulsman, H. A. B. Wösten and M. J. T. Reinders, *mBio*, 2015, **6**, e00111–e00115.
74 J. Lee, *Mycobiology*, 2011, **39**, 79–84.
75 S. Fischer-Parton, R. Parton, P. Hickey, J. Dijksterhuis, H. Atkinson and N. Read, *J. Microsc.*, 2000, **198**, 246–259.
76 J. Dijksterhuis and D. Molenaar, *Antonie van Leeuwenhoek*, 2013, **103**, 921–931.
77 M. Garduño-Rosales, O. A. Callejas-Negrete, E. Medina-Castellanos, S. Bartnicki-García, A. Herrera-Estrella and R. R. Mouriño-Pérez, *Fungal Genet. Biol.*, 2022, **159**, 103672.
78 G. J. Hageage and B. J. Harrington, *Lab. Med.*, 1984, **15**, 109–112.
79 W. Zhang, H. Yang, L. Jiang, L. Han and L. Wang, *J. Int. Med. Res.*, 2010, **38**, 1961–1967.
80 B. Chen, W. Li, Y. Pang, N. Zhang, S. Bian, C. Liu, Z. Yang, Y. Jiang, R. Li and Y. Xie, *J. Microbiol. Methods*, 2021, **184**, 106202.
81 F. Jiang, L. Zhang, J. Zhou, T. S. George and G. Feng, *New Phytol.*, 2021, **230**, 304–315.
82 C. E. Stanley, J. Shrivastava, R. Brugman, E. Heinzelmann, D. van Swaay and G. Grossmann, *New Phytol.*, 2018, **217**, 1357–1369.